

Observation and analysis of the center-of-mass position trajectory for trapped ultracold atoms

Zhi-Xin Duan(段志鑫), Ru-Fang Zhao(赵茹方), Wei-Tao Wu(吴炜韬), and Sheng-Jun Yang(杨胜军)
Citation: Chin. Phys. B, 2026, 35 (**8**): 083701. DOI: 10.1088/1674-1056/ae15f9
http://cpb.iphy.ac.cn; http://iopscience.iop.org/cpb

What follows is a list of articles you may be interested in

Atomic transport dynamics in crossed optical dipole trap

Peng Peng(彭鹏), Zhengxi Zhang(张正熙), Yaoyuan Fan(樊耀塬), Guoling Yin(殷国玲), Dekai Mao(毛德凯), Xuzong Chen(陈徐宗), Wei Xiong(熊炜), and Xiaoji Zhou(周小计)
Chin. Phys. B, 2024, 33 (**7**): 073701. DOI: 10.1088/1674-1056/ad401c

Efficient loading of cesium atoms in a magnetic levitated dimple trap

Guoqing Zhang(张国庆), Guosheng Feng(冯国胜), Yuqing Li(李玉清), Jizhou Wu(武寄洲), and Jie Ma(马杰)
Chin. Phys. B, 2024, 33 (**2**): 023702. DOI: 10.1088/1674-1056/ad0b03

Quantum degenerate Bose-Fermi atomic gas mixture of ^{23}Na and ^{40}K

Ziliang Li(李子亮), Zhengyu Gu(顾正宇), Zhenlian Shi(师振莲), Pengjun Wang(王鹏军), and Jing Zhang(张靖)
Chin. Phys. B, 2023, 32 (**2**): 023701. DOI: 10.1088/1674-1056/aca14f

Space continuous atom laser in one dimension

Yi Qin(秦毅), Xiao-Yang Shen(沈晓阳), Wei-Xuan Chang(常炜玄), and Lin Xia(夏林)
Chin. Phys. B, 2023, 32 (**1**): 013701. DOI: 10.1088/1674-1056/ac7861

Enhanced cold mercury atom production with two-dimensional magneto-optical trap

Ye Zhang(张晔), Qi-Xin Liu(刘琪鑫), Jian-Fang Sun(孙剑芳), Zhen Xu(徐震), and Yu-Zhu Wang(王育竹)
Chin. Phys. B, 2022, 31 (**7**): 073701. DOI: 10.1088/1674-1056/ac5397

Observation and analysis of the center-of-mass position trajectory for trapped ultracold atoms

Zhi-Xin Duan(段志鑫)[1,2], Ru-Fang Zhao(赵茹方)[1], Wei-Tao Wu(吴炜韬)[1], and Sheng-Jun Yang(杨胜军)[1,2,†]

[1] *Shenzhen Institute for Quantum Science and Engineering, School of Science, Southern University of Science and Technology, Shenzhen* 518055, *China*
[2] *International Quantum Academy, Shenzhen* 518048, *China*

(Received 13 September 2025; revised manuscript received 15 October 2025; accepted manuscript online 22 October 2025)

Optical dipole traps are indispensable tools in ultracold atomic physics, and precise understanding and control of atomic dynamics within the traps are critically important. Here, applying a magnetic gradient to perturb dipole-trapped ultracold atoms, we investigate the trajectory of the center of mass positions (CoMPs) when atoms are either in a single spin state ($|F=1,m_F=-1\rangle$) or in the pseudospin-mixed states ($|F=1,m_F=-1\rangle$ and $|F=1,m_F=0\rangle$). Unlike just treating the conventional time-of-flight (TOF) imaging as atomic momentum distribution, we present a methodology in-depth for accurate information about the atomic spatial trajectory evolution. This approach circumvents the need for complex and resource-intensive *in-situ* high-resolution imaging, broadening the accessibility of dynamic studies, and trap characterization across ultracold atoms. It can be directly used for fine-calibrating parameters of the trap potential and studying the atomic dynamical evolution, which will benefit various research areas of ultracold atoms.

Keywords: dipole-trapped ultracold atoms, center-of-mass position trajectory, gradient-field perturbation, spin mixture, spin dipole oscillation, spin drag

PACS: 37.10.Gh, 67.30.hj, 03.75.–b, 34.50.–s

DOI: 10.1088/1674-1056/ae15f9 **CSTR:** 32038.14.CPB.ae15f9

1. Introduction

Since ultracold atoms are prepared in vacuum chambers, they will expand in space with no trap and leave their original positions under gravity. Optical laser beams are the basic and most used tools for trapping and manipulating atoms, such as dipole trap,[1] tweezer,[2] and lattice,[3–5] to avoid unwanted atomic loss and meet long-term evolution requirements. In particular, the optical dipole trap is present in most ultracold atom experiments as a boundary box. The trapped atoms, involving various spin and gauge degrees of freedom, bring us numerous novel quantum phenomena, such as spin squeezing,[6–9] synchronization and chaos,[10–14] topology,[15–18] and superfluid phase transition.[19–23] In order to gain a deeper understanding and utilization of these topics, precise detection and control over atomic dynamics within the traps are important.

As is well known, for ultracold atom experiments, the primary detection method involves the time-of-flight (TOF) imaging of the atoms.[24–26] Due to the finite TOF time, the obtained image inevitably reflects the combined effect of atomic position and momentum distributions in the trap. Many existing approaches for characterizing the atomic motion roughly treat the TOF image as the atomic momentum distribution and only stay at analyzing their relative flying distances.[27–30] More precise *in-situ* spatial information often necessitates complex high-resolution imaging techniques.[31–33] These *in-situ* imaging methods, while powerful, often demand specialized and expensive equipment, potentially limiting their widespread adoption across all ultracold atom laboratories. The ability to achieve high precision with a comparatively simpler setup will lower the barriers for detailed dynamic studies, making the ultracold atom experiments more attainable for broader research.

Here, we revisit the physical picture and detection of dipole-trapped atoms in the ordinary TOF absorption imaging. The trajectory evolution of the center of mass positions (CoMPs) in the trap is obtained. It circumvents the need for complex numerical simulations involving computationally intensive Gross–Pitaevskii or Boltzmann equations, offering an accurate and efficient alternative for experimental analysis. This approach uniquely enables the detection of micrometer-scale position changes and atomic spatial trajectory evolution without the need for sophisticated *in-situ* imaging setups. The parameter noises that affect the trap stability can also be evaluated by monitoring the fluctuations of the CoMPs at a fixed moment.

In this paper, we present our model and experimentally demonstrate it by studying the CoMPs' trajectory that is perturbed by a gradient magnetic field. As shown in Fig. 1(a), the trapped ultracold atoms undergo oscillation when switching on an external force $F_\uparrow$ which induces an additional tilted potential. In addition, a spin mixture (pseudospin-half $f=1/2$)

†Corresponding author. E-mail: yangsj@sustech.edu.cn

© 2026 Chinese Physical Society and IOP Publishing Ltd. All rights, including for text and data mining, AI training, and similar technologies, are reserved.

is investigated in the case that the external force only perturbs one of the two spin components. Analogous to Coulomb drag,[34] the spin drag effect for Bose gases is expected to occur.[35,36] As illustrated in Fig. 1(b), an external force $F_\uparrow$ drives the spin-up component to oscillate in the trap. Though the external force $F_\downarrow$ is zero, the spin-down component will be dragged to oscillate due to momentum-exchange scattering. Reciprocally, it will dampen the oscillation of the spin-up component. The spin drag and damping effects are preliminarily investigated by modifying the population distribution of the two spin states and analyzing their CoMPs' trajectory via our method. As shown below, the experimental data are well consistent with our theoretical calculations.

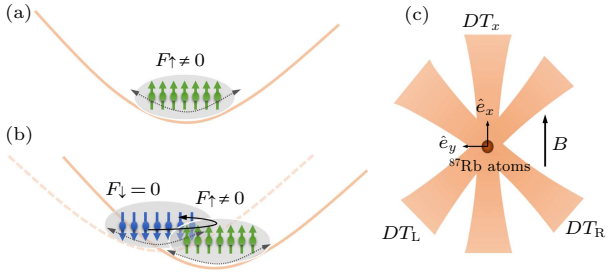


Fig. 1. (a) Trapped atoms in the single spin-up state $|\uparrow\rangle$ (green) undergo harmonic oscillation driven by an external force $F_\uparrow$. (b) Atomic spin oscillation and drag in a trap, where only the spin-up atoms ($|\uparrow\rangle$) are perturbed by the external force ($F_\uparrow \neq 0$ and $F_\downarrow = 0$). (c) Schematic setup, where three crossed laser beams (DT_x, DT_R, and DT_L) in the $\hat{e}_x$–$\hat{e}_y$ plane are used to form the dipole trap for ultracold ^{87}Rb atoms. The bias magnetic field B is in the $\hat{e}_x$ direction.

2. Setup and model description

Our setup is shown in Fig. 1(c). Three laser beams (with the wavelength $\lambda = 1064$ nm) that intersect horizontally are used to create the dipole trap. The two beams DT_L and DT_R are symmetrically arranged with the angle around $\pm 45^\circ$ relative to the $\hat{e}_x$ axis. They form a crossed dipole trap, which is also used for evaporative cooling of the atoms. The horizontal beam waist σ_h for the trap is 180 μm. The vertical beam waist σ_v is smaller compared with σ_h, with a value of 55 μm, which counteracts the influence of gravity with an acceptable laser power requirement and benefits the evaporative cooling. The vertical trapping frequency ω_z is larger than the horizontal trapping frequencies. Restricting the atomic motion in the $\hat{e}_x$–$\hat{e}_y$ plane, the crossed trap can be simplified as $M\omega_\mathrm{L}^2(x-y)^2/4 + M\omega_\mathrm{R}^2(x+y)^2/4$, where M is the mass of rubidium atom, ω_L and ω_R are the radial trapping frequencies of the beams DT_R and DT_L. The crossed dipole trap allows us to study the two-dimensional (2D) oscillator in the horizontal plane. The third beam DT_x is in the $\hat{e}_x$ direction with its beam waist radius $\sigma_x \sim 120$ μm. The intensity of this beam is larger than the other two. It is used to confine atomic motion in the $\hat{e}_y$ direction and modify the profile of the dipole trap. The three beams work together to enable us to study the one-dimensional (1D) oscillator along the $\hat{e}_x$ direction.

In the experiments, the spin-up state $|\uparrow\rangle$ and the spin-down state $|\downarrow\rangle$ are the ^{87}Rb ground levels $|F=1, m_F=-1\rangle$ and $|F=1, m_F=0\rangle$, respectively. They form a pseudospin-half ($f=1/2$) system. Initially, ultracold atoms are prepared in the crossed dipole trap of the two beams DT_L and DT_R, containing a total of $\sim 2\times 10^5$ atoms in the state $|\uparrow\rangle$. The atomic temperature is 30 nK, and the size of the atomic cloud is about 28 μm. The vast majority of the atoms are in the condensed phase. A bias magnetic field B, with the strength of 10.58 Gs (1 Gs = 10^{-4} T), is applied horizontally along the $\hat{e}_x$ direction as the quantization axis. One resonant radio-frequency (rf) pulse is applied to transfer atoms between the two states $|F=1, m_F=-1\rangle$ and $|F=1, m_F=0\rangle$. Further transfer to the state $|F=1, m_F=+1\rangle$ is significantly suppressed due to the quadrature Zeeman effect. Thus, unlike those experiments carried out under a weak magnetic field,[37,38] atoms in the sublevel $|F=1, m_F=0\rangle$ cannot scatter into atoms in the $|F=1, m_F=+1\rangle$ and $|F=1, m_F=-1\rangle$ states for our system. There is no involvement of unwanted spin-exchange collision and spin precession. Without pumping from external fields, such as the rf pulse, the population of the two spin components is maintained.

As the spin-up state $|\uparrow\rangle$ is magnetically sensitive and the spin-down state $|\downarrow\rangle$ is magnetically insensitive, we apply a gradient field $B'x\hat{e}_x + B'y\hat{e}_y - 2B'z\hat{e}_z$ to create the external force $F_\uparrow$ and perturb the spin-up atoms while the spin-down atoms have no influence. B' is the gradient strength, with a value of around 1 Gs/cm in our experiments. The contributed field disturbance over the atoms is on the level of mGs, about four orders of magnitude smaller than the bias field B. Thus, the bias field is maintained as a good quantization axis. The total magnetic field can be simplified as $(B + B'x)\hat{e}_x$. Atoms are prepared either purely in the state $|\uparrow\rangle$ or coexist in the two states $|\uparrow\rangle$ and $|\downarrow\rangle$, and then perturbed by switching on the gradient field B' for evolution observation, as depicted in Figs. 1(a) and 1(b).

The evolution of the trapped atoms is measured by the TOF absorption imaging. It is done by abruptly switching off the trap after an evolution time t since switching on the gradient field B'. Then, after a freely expanding time $T = 25$ ms, we use a camera to image the atomic distribution in the $\hat{e}_x$–$\hat{e}_y$ plane. The gradient field remains open during the TOF process. The averaged position (x_0^*, y_0^*) for atomic distribution in the TOF image when $t = 0$ ms is calibrated as the reference zero point. Then, for each absorption image, the averaged atomic position can be obtained as

$$\langle r^*(t)\rangle = \sum \hat{r}\cdot(x^*, y^*; t)\frac{n(x^*, y^*; t)}{N}, \tag{1}$$

where $n(x^*, y^*; t)$ is the atomic number at the point (x^*, y^*), N is the total atomic number, and $\hat{r}$ is the calculated projection direction, t is the evolution time in the trap. The variance

$\delta r^*(t) = \sqrt{\langle r^{*2}(t)\rangle - \langle r^*(t)\rangle^2}$ can also be calculated. The time-varying value $\langle r^*(t)\rangle$ is related to the atomic CoMPs in the trap. Treating the trap as a harmonic potential in the $\hat{r}$ direction, the additional velocity for the atoms due to the trap is $\omega_r r(t)$ where ω_r is the trapping frequency. According to the relation $r(t)+\omega_r r(t)T = r^*(t)$, we estimate the atomic CoMPs in the trap as

$$\bar{r}(t) = \frac{\langle r^*(t)\rangle}{\chi\omega_r T}, \tag{2}$$

where $\chi = (1+\omega_r T)/\omega_r T$ is the correction factor. χ is approaching 1 when $\omega_r T \gg 1$, where the trap is tight and the flying time is long. Meanwhile, assuming a normal distribution for simplicity, the position deviation $\Delta r(t)$ can be obtained as

$$\Delta r(t) = \frac{\sqrt{2}\delta r^*(t)}{\chi\omega_r T}, \tag{3}$$

which reflects the size of the atomic cloud in the trap.

Considering the actual situation that the laser beam employed has a Gaussian profile, the trap potential is labeled as $U(r;r_0,\sigma_r) := U_0 \exp\left[-2(r-r_0)^2/\sigma_r^2\right]$. $r_0 = 0$ is the central position, σ_r is the beam waist, and U_0 is the trap depth. The trap can be expanded in Taylor series as $(2U_0/\sigma_r^2)r^2\left(1 - O\left(r^2/\sigma_r^2\right)\right)$, where $O\left(r^2/\sigma_r^2\right) \simeq (r^2/\sigma_r^2)\left(1-2r^2/3\sigma_r^2\right)$ is the higher-order correction. It is simplified as a harmonic potential when r is small compared with σ_r. The trapping frequency ω_r equals $2\sqrt{U_0/M}(1/\sigma_r)$. Considering higher-order correction, the trapping frequency ω_r is replaced with $\omega_r\sqrt{1-r^2/\sigma_r^2}$. Iteratively correcting the results in Eq. (2), the value of the atomic CoMPs is then modified as

$$\bar{r}_{\rm corr}(t) \simeq \frac{\bar{r}(t)}{1-\dfrac{1}{\chi}\dfrac{\bar{r}^2(t)}{2\sigma_r^2}} \simeq \bar{r}(t)\left(1+\frac{1}{\chi}\frac{\bar{r}^2(t)}{2\sigma_r^2}\right). \tag{4}$$

The weight of the correction is determined by σ_r, and is about one-tenth when $\bar{r}(t)$ is less than half of σ_r. This indicates that the correction is small if the excursion from the equilibrium position is small with respect to the beam waist, and the harmonic approximation is good enough. For more accuracy, we use Eq. (4) for measurement analysis. As demonstrated below, our model allows us to have a clear understanding of both the trap potential and the trapped atomic motion.

3. One-dimensional case

First, we conducted measurements and verification for the 1D oscillation along the quantization axis. After preparing purely spin-up atoms in the crossed dipole trap of the two beams $DT_{\rm L}$ and $DT_{\rm R}$, the third beam DT_x is linearly switched on within 50 ms. After holding atoms in the trap for another 50 ms, the gradient field B' is switched on to drive the atomic pendulum movement. Then, waiting for an evolution time t, we switch off the trap for the TOF imaging in the $\hat{e}_x$–$\hat{e}_y$ plane. Together with the three laser beams, the trap potential can be approximately written as $V_{\rm DT} = M\omega_x^2x^2/2 + M\omega_y^2y^2/2 + M\omega_z^2z^2/2$. $\{\omega_x,\omega_y\}$ is the horizontal trapping frequencies with the calibrated values of $2\pi\times 25$ Hz and $2\pi\times 67$ Hz. The vertical trapping frequency ω_z has not been directly measured, and its estimated value is $2\pi\times 130$ Hz. Atomic motion perturbed by the gradient field B' is along the quantization axis $\hat{e}_x$. We simply treat it as a 1D oscillator, that $V_{\rm DT} = M\omega_x^2x^2/2$.

Results of the CoMPs' trajectory $(\bar{x}(t),\bar{y}(t))$ (black data and red line) are presented in the upper part of Fig. 2(a), where $t\in[0,200]$ ms with a step of $\Delta t = 2$ ms. The gradient B' is set at 1.1 Gs/cm. Atomic oscillation occurs in the $\hat{e}_x$ direction. $X_0 = 0$ μm is the initial position when $t = 0$ ms, and $X_{\rm c} = 2.6\pm0.1$ μm is the central position of the oscillation. The measured trajectory in Fig. 2(a) is obtained by finely adjusting the intersection of the three beams $DT_{\rm L}$, $DT_{\rm R}$, and DT_x. Oscillation in the $\hat{e}_y$ direction is reduced to a negligible level. To achieve this, the key point is that the beam DT_x is in the $\hat{e}_x$ direction and its axis passes through the intersection center of the other two beams $DT_{\rm L}$ and $DT_{\rm R}$. Otherwise, oscillation will occur in the $\hat{e}_y$ direction. An example without proper adjustment is plotted in light blue for comparison. In the lower part of Fig. 2(a), the atomic CoMPs $\bar{x}(t)$ along the $\hat{e}_x$ direction are fitted with the sinusoidal damping function. The dashed line labels the oscillation central position $X_{\rm c} = 2.6$ μm. The fitting amplitude A_x equals 30.3±0.6 μm. It decays slowly with time. We owe the decay to collision dissipation due to the thermal atoms[39] and light-induced thermal effects on the atoms. To verify this, according to Eq. (3), we calculate the size of the atomic cloud Δx in Fig. 2(b). The value of Δx is consistent with the Thomas–Fermi radius. As expected, the cloud is expanding. Linearly fitting, Δx increases by about 12 μm/s.

Theoretically, the force $F_\uparrow$ induces the position displacement d_x of the potential minima equaling

$$\frac{\mu_{\rm B}B'}{2M\omega_x^2}, \tag{5}$$

where $\mu_{\rm B}$ is the Bohr magneton. According to the experimental parameters, the calculated displacement d_x equals 14.3 μm. We estimate the potential bottom of the dipole trap at around the dot–dashed line $\bar{x} = -11.7$ μm in Fig. 2(a). In the actual experiment, the gradient field B' is switched on with a time of about 2 ms. At the initial $t = 0$ ms, the dipole trap is switched off while the gradient has not been fully applied. The measured position is away from the dot–dashed line and does not follow the sinusoidal fitting trajectory. The atoms undergo some adiabatic evolution during the rising time of B'. The effective position displacement d_x is corrected as

$$d_{x,\rm cor} = \frac{\mu_{\rm B}B'}{2M\omega_x^2}(1-\sin(\omega_x\tau)), \tag{6}$$

where $\tau = 2$ ms. It reflects the actual energy changes of the Bose gas from the initial stage to the new equilibrium position. The value of $d_{x,\mathrm{cor}}$ is obtained to be 9.9 μm, equaling the distance between the dashed and dotted lines in Fig. 2(a). Furthermore, based on $M\omega_x^2 A_x^2/2 = M\omega_x^2 d_x^2/2 + F_\uparrow(A_x + d_x)$, the oscillation amplitude A_x is expected to be three times $d_{x,\mathrm{cor}}$. It equals 29.7 μm, consistent with the measured result of 30.3 μm.

After checking the gradient-field perturbed oscillation of the spin-up atoms, we turn to study the spin drag and damping effect when atoms coexist in the two states $|\uparrow\rangle$ and $|\downarrow\rangle$. The atoms are initially prepared in the state $|\uparrow\rangle$. The rf pulse is applied to adjust the population distribution. Then, the gradient field B' is switched to perturb the evolution of the spin mixture. B' is still set at 1.1 Gs/cm. To obtain their individual distributions, we apply a strong gradient field (~ 8 Gs/cm) during the TOF process to completely separate the two components. Figure 3 shows the measured results with three different populations, $\eta = N_\downarrow/N = \{0.3, 0.5, 0.7\}$. $N_\downarrow$ is the atom number in the state $|\downarrow\rangle$. As shown in Figs. 3(a1)–3(a3), both the two components' CoMPs, $\bar{x}_\uparrow$ in black and $\bar{x}_\downarrow$ in red, oscillate with time. The gray-line data are for reference where $\eta = 0$. When $t \simeq 13$ ms, $\bar{x}_\uparrow$ for the spin-up atoms reaches its maximum. Considering the cloud size of the atoms, the two components are almost entirely separated at this momentum. At around 25 ms, the spin-up atoms return to collide with the spin-down atoms. The spin-down atoms are dragged to oscillate. For large η, the oscillation of $\bar{x}_\uparrow$ reverses faster after collision with the spin-down atoms. It is easy to understand because more spin-down atoms increase the momentum exchange rate for the spin-up atoms and prevent them from passing through.

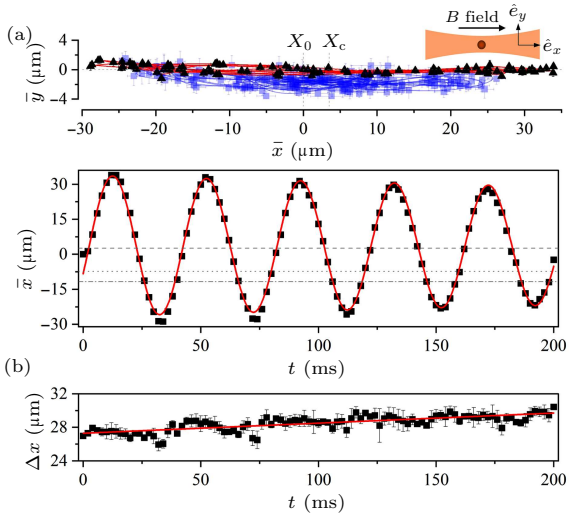


Fig. 2. (a) Evolution of the CoMPs for the 1D trapped ^{87}Rb atoms, where $B' = 1.1$ Gs/cm. Upper part: the averaged trajectory $(\bar{x}, \bar{y})$ (black data and red line) in the $\hat{e}_x$–$\hat{e}_y$ plane. $X_0 = 0$ μm and $X_c = 2.6$ μm are the starting and central positions of the oscillation. For comparisons, the light blue data is a measurement result with improper adjustment of the three laser beams. Lower part: the damped sinusoidal fitting of $\bar{x}$. t is the evolution time after switching on B', with step of 2 ms. The dashed, dotted, and dot–dashed lines represent the value $\bar{x}$ of 2.6 μm, −7.3 μm, and −11.7 μm, respectively. (b) The corresponding atomic cloud size Δx in the $\hat{e}_x$ direction. The slope is about 12 μm/s for linear fitting.

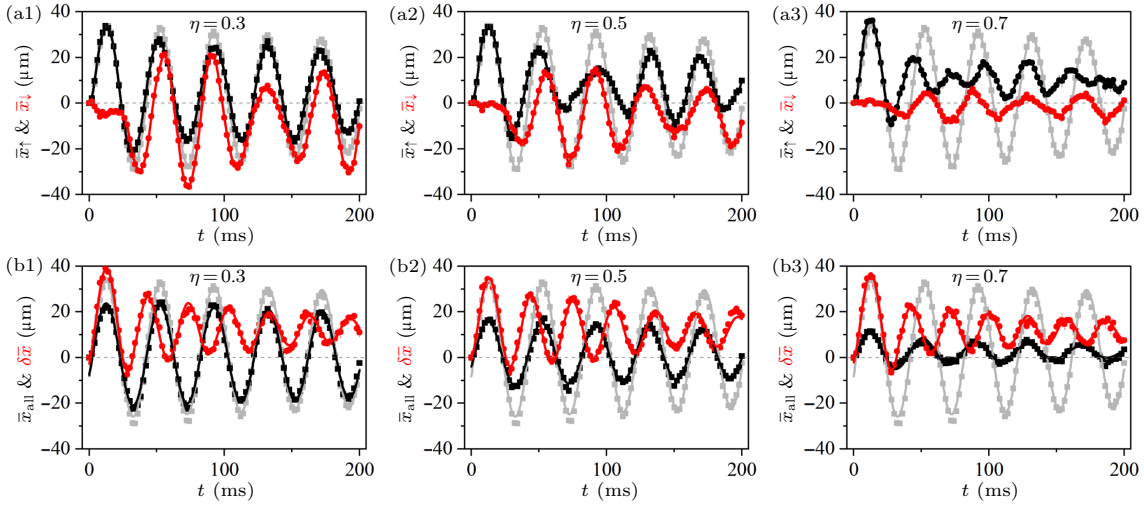


Fig. 3. Trajectory evolution of the CoMPs for the 1D case when atoms coexist in the states $|\uparrow\rangle$ ($|F = 1, m_F = -1\rangle$) and $|\downarrow\rangle$ ($|F = 1, m_F = 0\rangle$). Three population settings of $\eta = N_\downarrow/N$ at 0.3, 0.5, and 0.7 are present. $N_\downarrow$ is the number of the spin-down atoms, and N is the total atomic number. Subfigures (a1)–(a3) represent the CoMPs for each component in the $\hat{e}_x$ direction, where $\bar{x}_\uparrow$ (black square) and $\bar{x}_\downarrow$ (red) correspond to the trajectory of the spin-up and spin-down components, respectively. Subfigures (b1)–(b3) show the global oscillation of the CoMPs $\bar{x}_{\mathrm{all}}$ (black square) for all the atoms and the relative distance $\delta\bar{x}$ (red) between $\bar{x}_\uparrow$ and $\bar{x}_\downarrow$. The gray-line data ($\eta = 0$) are plotted for reference.

For small η, spin synchronous oscillation is well established via the interparticle interactions between the two components. When η becomes large, their oscillations seem irregular. To see more clearly, we calculate their averaged CoMPs $\bar{x}_{\mathrm{all}}$ ($:= (1-\eta)\bar{x}_\uparrow + \eta\bar{x}_\downarrow$, black square) and relative distance δx ($:= \bar{x}_\uparrow - \bar{x}_\downarrow$, red circle) in Figs. 3(b1)–3(b3) accordingly. Both $\bar{x}_{\mathrm{all}}$ and δx oscillate regularly but with different periods. It is a bang-bang interaction between the two components. The oscillation curve of $\bar{x}_{\mathrm{all}}$ deviates at the rising and falling directions from the sinusoidal function, especially for large η. It just originates from the motion resistance of the spin-down atoms. The amplitude of $\bar{x}_{\mathrm{all}}$ reflects the perturba-

tion due to the gradient B', thus proportional to the atomic population in the spin-up state $|\uparrow\rangle$. It becomes small for large η. The separation distance δx reflects the spin dipole oscillation. Unlike observation in the spin-1 system that exists opposite-driving components,[29,40] the oscillation here is faster than the frequency ω_x since the spin-down atoms have no externally driven force but are collided with and dragged by the spin-up atoms. δx decays slowly to a non-zero equilibrium point $\delta\bar{x}_0 \simeq 15.5 \pm 0.4$ μm for $\eta = 0.5$, which reflects the distance between the two components' potential minima. It is consistent with the theoretical estimation of $d_x = 14.3$ μm as discussed above.

4. Two-dimensional case

Next, we discuss the more general and complex two-dimensional (2D) oscillation. It is done by removing the beam DT_x and retaining the other two beams DT_L and DT_R. As shown in Fig. 4(a), the beams DT_L and DT_R are in the $\hat{e}_\mathrm{L}$ and $\hat{e}_\mathrm{R}$ directions. The trapping frequencies along the two directions are $\omega_\mathrm{L} = 2\pi \times 29$ Hz and $\omega_\mathrm{R} = 2\pi \times 24$ Hz, respectively. All the atoms are prepared in the spin-up state $|\uparrow\rangle$. Still, the bias field B is 10.58 Gs and the gradient field B' equals 1.1 Gs/cm. Figure 4(a) shows the oscillating trajectory of the atomic CoMPs $(\bar{x}, \bar{y})$ during the time $t \in [0, 200]$ ms. For clarity, the data line after 100 ms is displayed in light red. The trajectory reflects the profile of the 2D trap potential. Based on the trajectory boundary, we obtain the two beams' accurate directions $\hat{e}_\mathrm{L}$ and $\hat{e}_\mathrm{R}$ with the angles of $\theta_\mathrm{L} = 48.5°$ and $\theta_\mathrm{R} = 52.5°$ to the $\hat{e}_x$ direction. $(X_0 = 0\ \mu\mathrm{m}, \mathrm{Y}_0 = 0\ \mu\mathrm{m})$ in Fig. 4(b) is the start point. The blue arrow indicates the moving direction of the atom cloud. The atomic CoMPs $(\bar{x}, \bar{y})$ undergoes centrifugal rotation. During the 200-ms evolution time, the CoMPs $(\bar{x}, \bar{y})$ first rotate clockwise and then turn to rotate counterclockwise. The oscillation amplitude A_R in the $\hat{e}_\mathrm{R}$ direction is higher than the amplitude A_L in the $\hat{e}_\mathrm{L}$ direction, which is as expected since it is inversely proportional to the square of the trapping frequency.

We calculate and sinusoidally fit the temporal evolution of the atomic CoMPs along the two directions in Fig. 4(b). The CoMPs $\bar{r}\cdot\hat{e}_\mathrm{L}$ (black square) and $\bar{r}\cdot\hat{e}_\mathrm{R}$ (red circle) undergo periodic sinusoidal oscillations. Here, $\bar{r}$ is the displacement vector of the CoMPs relative to the initial position (X_0, Y_0). The fitting results of the central positions and oscillation amplitudes are -10.0 ± 0.3 μm and 15.1 ± 0.5 μm in the $\hat{e}_\mathrm{L}$ direction, and 14.1 ± 0.2 μm and 26.7 ± 0.3 μm in the $\hat{e}_\mathrm{R}$ direction. According to the fitting results, the blue dot in Fig. 4(a) labels the oscillation central position $(X_\mathrm{c} = 2.7\ \mu\mathrm{m}, \mathrm{Y_c} = 15.7\ \mu\mathrm{m})$. Based on theoretical calculation, we infer that the potential bottom of the dipole trap is located close to the green circle point $(\bar{x} = -14\ \mu\mathrm{m}, \bar{y} = 12\ \mu\mathrm{m})$. Similar to the 1D case, the atomic CoMPs in the initial stage are away from the green point due to the 2-ms rising time of the gradient B'. According to the equation $A_i = \frac{3\mu_\mathrm{B}B'}{2M\omega_i^2}\frac{\sin\theta_i}{\sin(\theta_\mathrm{L}+\theta_\mathrm{R})}(1-\sin(\omega_i\tau))$ where $i = \{\mathrm{L}, \mathrm{R}\}$, we obtain the theoretical oscillation amplitudes A_L and A_R equal 16.2 μm and 27.8 μm, respectively. They are very close to the experimental results 15.1 μm and 26.7 μm. The results are plotted in Fig. 4(c), together with measurements for some other gradient strengths of B' between 0.3 Gs/cm and 1.5 Gs/cm. The solid and dashed lines are the linear fits of the experimental results and the theoretical calculations, respectively. The slopes for the linear fitting of A_L and A_R are 13.9 ± 0.4 μm and 25.9 ± 0.5 μm per Gs/cm. The corresponding theoretical values are 14.7 μm and 25.3 μm per Gs/cm, which are basically consistent with the measured results.

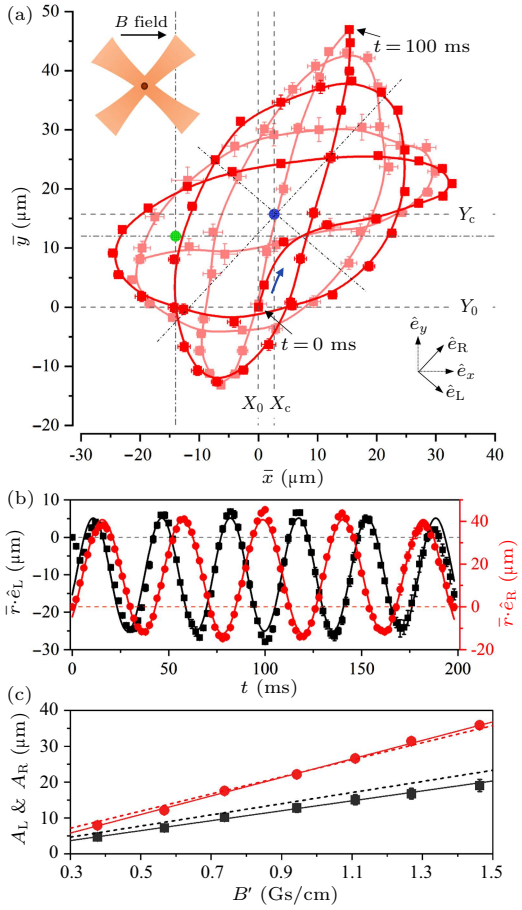


Fig. 4. (a) Oscillation trajectory of the atomic CoMPs $(\bar{x}, \bar{y})$ in the 2D case. Atoms are in the spin-up state $|\uparrow\rangle$, B' is 1.1 Gs/cm, the red (light red) data line corresponds to the time $t = [0, 100]$ ms ($[100, 200]$ ms), (X_0, Y_0) is the start point, the blue point $(X_\mathrm{c}, Y_\mathrm{c})$ is the oscillation central position, the green point is the estimated dipole trap minina. (b) The corresponding CoMPs $\bar{r}\cdot\hat{e}_\mathrm{L}$ (black square) and $\bar{r}\cdot\hat{e}_\mathrm{R}$ (red circle), where $\bar{r} = (\bar{x}, \bar{y})$; (c), Oscillation amplitudes A_i for different gradient B', where $i = \{\mathrm{L}, \mathrm{R}\}$ represent the $\hat{e}_\mathrm{L}$ and $\hat{e}_\mathrm{R}$ direction, the solid and dashed lines are the linearly fitting and theoretical results, respectively.

Furthermore, we check the subsequent motion of the atoms by removing the force $F_\uparrow$. Instead of switching off B', it is done by rf-pumping atoms to the spin-down state $|\downarrow\rangle$ after a specific evolution time t_p for the spin-up state $|\uparrow\rangle$ since the gradient field is on. The rf π-pulse is about tens of μs. The atomic positions remain unchanged during the pumping process. In Figs. 5(a)–5(c), three cases are shown for comparisons where

the rf pulse is switched on at the time $t_p = \{6, 20, 32\}$ ms accordingly. Parameter settings of the dipole trap and magnetic field are the same as the settings in Fig. 4(a). The purple arrows label the starting position when pumping atoms to the spin-down state $|\downarrow\rangle$. The trajectories maintain left and right rotating oscillation. Due to the existence of the gradient field, the trap potentials for the two spin states have some spatial differences, and the atomic energy is altered before and after the rf-pumping pulse. The oscillation amplitudes reflect the combined effect of the gradient field and the rf pulse. In Fig. 5(d), we plot the oscillation amplitudes A_L (black square) and A_R (red circle) for different t_p. The dashed lines are the reference amplitude obtained in Fig. 4(b). Initially, the amplitude increases with the time t_p. It reaches the maximum when $t_p \simeq 20$ ms. At this moment, the atoms are roughly located in the shift direction of the central position (X_c, Y_c) from the green dot, as seen in Fig. 4(a). For larger t_p, the oscillation amplitude decreases as the CoMPs $(\bar{x}, \bar{y})$ move in the opposite direction.

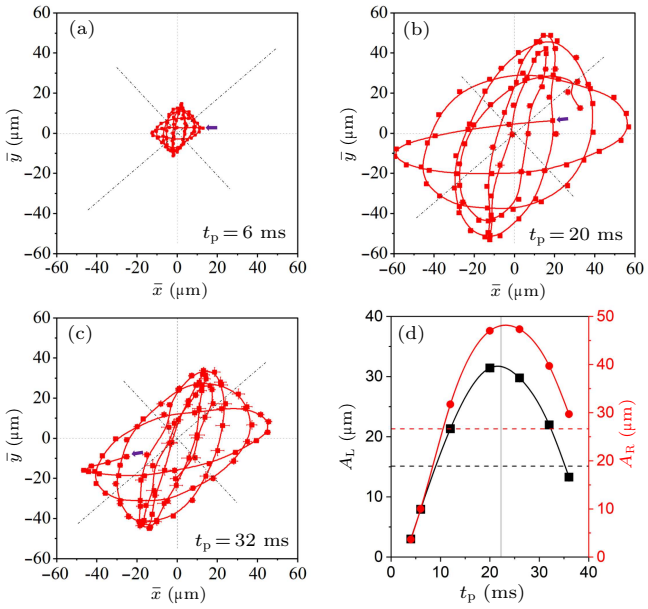


Fig. 5. (a)–(c) Evolution trajectory of the atomic CoMPs $(\bar{x}, \bar{y})$ after all the atoms are pumped from the spin-up state $|\uparrow\rangle$ to the spin-down state $|\downarrow\rangle$. $t_p = \{6, 20, 32\}$ ms are the evolution times for the spin-up atoms before the rf pumping, and the purple arrows indicate the starting position when switching on the rf pulse. Parameter settings of the dipole trap and magnetic field are the same as the settings in Fig. 4(a). (d) Oscillation amplitudes A_L (black square) and A_R (red circle) for different times t_p, where the dashed lines are the amplitude values that were measured in Fig. 4(b).

For the 2D case, we also conduct the spin drag measurement when the two spin components coexist (Fig. 6). The gradient field B' is 1.1 Gs/cm. Figures 6(a)–6(c) show the evolution trajectory both for the spin-up (black) and spin-down (red) components when setting the proportion $\eta = \{0.3, 0.5, 0.7\}$. The spin-up atoms initially separate from the spin-down atoms and then return to collide with the spin-down atoms. The oscillation amplitude decreases as η increases. Their relative distance d changing over time is calculated in Fig. 6(d). Since ω_L and ω_R are unequal, the results of d are a bit more complex than the measured $\delta\bar{x}$ of the 1D case in Fig. 3. The dashed line shows the averaged distance value of 21.8 μm. It reflects the separation of the trap minima between the two spin components.

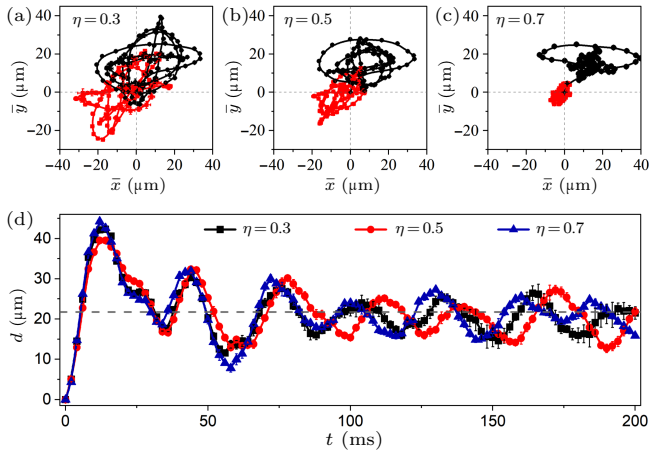


Fig. 6. Evolution trajectory of the atomic CoMPs $(\bar{x}, \bar{y})$ for the 2D oscillation when atoms coexist in the spin-up state $|\uparrow\rangle$ (black) and the spin-down state $|\downarrow\rangle$ (red). (a)–(c) Three cases of the atomic populations η at 0.3, 0.5, and 0.7 are shown for comparisons. (d) The corresponding relative distance d between the two components' CoMPs. The dashed line is the averaged value of d and is equal to 21.8 μm.

Since the scattering rate for atoms in one spin state is proportional to the density of atoms in the other state, atoms with a smaller population are more susceptible to following the movement of atoms with a larger population. Compared with the balanced distribution $\eta = 0.5$, the motion of the spin-down (spin-up) atoms is more likely to be dragged (damped) by the spin-up (spin-down) atoms when $\eta = 0.3$ ($\eta = 0.7$). As observed, the distance d changes faster for unbalanced distributions ($\eta \neq 0.5$). The relative distance of the CoMPs seems to be a good parameter for the study of the spin drag effect.

5. Conclusion

In this paper, we studied gradient magnetic-field perturbed oscillation of the ultracold ^{87}Rb atoms in an optical dipole trap. A reasonable calculation model is presented for analysis of the atomic CoMPs based on the fundamental law of energy and momentum conservation. The trajectory evolution of the atomic CoMPs is extensively investigated using conventional TOF absorption imaging instead of *in-situ* high-resolution imaging. The experimental results are well consistent with our theoretical calculations. Our results should be valuable for accurate calibration of the trapping system, observation of the atomic dynamical evolution, and measurement of external forces such as gravity or gradient magnetic fields, which should benefit plenty of future research on trapped ultracold atoms.

Acknowledgements

Project supported by the Key-Area Research and Development Program of Guangdong Province, China (Grant No. 2019ZT08X324) and the Fund from Guangdong Provincial Key Laboratory (Grant No. 2019B121203002).

References

[1] Grimm R, Weidemüller M and Ovchinnikov Y B 2000 *Adv. Atom Mol. Opt. Phys.* **42** 95
[2] Kaufman A M and Ni K K 2021 *Nat. Phys.* **17** 1324
[3] Bloch I and Zoller P 2012 *Contemp. Concepts Condens. Matter Sci.* **5** 121
[4] Gross C and Bloch I 2017 *Science* **357** 995
[5] Schäfer F, Fukuhara T, Sugawa S, Takasu Y and Takahashi Y 2020 *Nat. Rev. Phys.* **2** 411
[6] Gross C 2012 *J. Phys. B: At. Mol. Opt. Phys.* **45** 103001
[7] Bilitewski T, Marco D L, Li J R, Matsuda K, Tobias W G, Valtolina G, Ye J and Rey A M 2021 *Phys. Rev. Lett.* **126** 113401
[8] Huang M Z, de la Paz J A, Mazzoni T, Ott K, Rosenbusch P, Sinatra A, Garrido Alzar C L and Reichel J 2023 *PRX Quantum* **4** 020322
[9] Zhang T, Maiwöger M, Borselli F, Kuriatnikov Y, Schmiedmayer J and Prüfer M 2024 *Phys. Rev. X* **14** 011049
[10] Qiu H, Zambrini R, Polls A, Martorell J and Juliá-Díaz B 2015 *Phys. Rev. A* **92** 043619
[11] Dogra N, Landini M, Kroeger K, Hruby L, Donner T and Esslinger T 2019 *Science* **366** 1496
[12] Laskar A W, Adhikary P, Mondal S, Katiyar P, Vinjanampathy S and Ghosh S 2020 *Phys. Rev. Lett.* **125** 013601
[13] Duong Anh-Tai T, Mikkelsen M, Busch T and Fogarty T 2023 *SciPost Phys.* **15** 048
[14] Kim J, Jung J, Lee J, Hong D and Shin Y 2024 *Phys. Rev. Res.* **6** L032030
[15] Goldman N, Budich J C and Zoller P 2016 *Nat. Phys.* **12** 639
[16] Zhang D W, Zhu Y Q, Zhao Y X, Yan H and Zhu S L 2018 *Adv. Phys.* **67** 253
[17] Cooper N R, Dalibard J and Spielman I B 2019 *Rev. Mod. Phys.* **91** 015005
[18] Braun C, Saint-Jalm R, Hesse A, Arceri J, Bloch I and Aidelsburger M 2024 *Nat. Phys.* **20** 1306
[19] Greiner M, Mandel O, Esslinger T, Hänsch T W and Bloch I 2002 *Nature* **415** 39
[20] Stamper-Kurn D M and Ueda M 2013 *Rev. Mod. Phys.* **85** 1191
[21] Zhu Q Z and Wu B 2015 *Chin. Phys. B* **24** 050507
[22] Baroni C, Lamporesi G and Zaccanti M 2024 *Nat. Rev. Phys.* **6** 736
[23] Zheng Y G, Luo A, Shen Y C, He M G, Zhu Z H, Liu Y, Zhang W Y, Sun H, Deng Y, Yuan Z S and Pan J W 2025 *Nat. Phys.* **21** 208
[24] Zhang H C, Zhang P F, Xu X P, Cheng F and Wang Y Z 2009 *Opt. Commun.* **282** 3278
[25] Zaleski T A and Kopeć T K 2011 *Phys. Rev. A* **84** 053613
[26] Hueck K, Luick N, Sobirey L, Siegl J, Lompe T, Moritz H, Clark L W and Chin C 2017 *Opt. Express* **25** 8670
[27] Eto Y, Sadgrove M, Hasegawa S, Saito H and Hirano T 2014 *Phys. Rev. A* **90** 013626
[28] Luo X, Wu L, Chen J, Guan Q, Gao K, Xu Z F, You L and Wang R 2016 *Sci. Rep.* **6** 18983
[29] Kim J H, Seo S W and Shin Y 2017 *Phys. Rev. Lett.* **119** 185302
[30] Tian L, Zheng N, Jian J, Liu W, Wu J, Li Y, Fu Y, Li P, Sovkov V, Ma J, Xiao L T and Jia S T 2022 *Chin. Phys. B* **31** 110302
[31] Ott H 2016 *Rep. Prog. Phys.* **79** 054401
[32] Gross C and Bakr W S 2021 *Nat. Phys.* **17** 1316
[33] Su L, Douglas A, Szurek M, Hébert A H, Krahn A, Groth R, Phelps G A, Marković O and Greiner M 2025 *Nat. Commun.* **16** 1017
[34] Narozhny B N and Levchenko A 2016 *Rev. Mod. Phys.* **88** 025003
[35] Duine R A and Stoof H T C 2009 *Phys. Rev. Lett.* **103** 170401
[36] van Driel H J, Duine R A and Stoof H T C 2010 *Phys. Rev. Lett.* **105** 155301
[37] Chang M S, Hamley C D, Barrett M D, Sauer J A, Fortier K M, Zhang W, You L and Chapman M S 2004 *Phys. Rev. Lett.* **92** 140403
[38] Chang M S, Qin Q, Zhang W, You L and Chapman M S 2005 *Nat. Phys.* **1** 111
[39] Fava E, Bienaimé T, Mordini C, Colzi G, Qu C, Stringari S, Lamporesi G and Ferrari G 2018 *Phys. Rev. Lett.* **120** 170401
[40] Bienaimé T, Fava E, Colzi G, Mordini C, Serafini S, Qu C, Stringari S, Lamporesi G and Ferrari G 2016 *Phys. Rev. A* **94** 063652